Chapter

Lifting Entry Analysis for Manned Mars Exploration Missions

Andrea Aprovitola, Fabrizio Medugno, Giuseppe Pezzella, Luigi Iuspa and Antonio Viviani

Abstract

In the present work, a feasibility study of a manned Mars entry, descent, and landing mission, performed with a lifting vehicle, is analyzed. Mars entry challenges relate to different atmosphere models; consequently, the effective landing capability of a winged configuration is discussed. An entry trajectory study in the Martian atmosphere assuming both a planar and non-planar three degree-of-freedom model is performed. Peak heat rates and time-integrated heat loads during the descent are computed verifying the entry corridor. It is shown that prescribed aerodynamic performances can be modulated explicitly by varying angle of attack and implicitly with bank-angle modulation. Finally, the resulting trajectory is discussed in terms of g-loads, total range performances, and integral heat load absorbed, in the perspective of future manned exploration missions.

Keywords: lifting body, Mars entry aerodynamics, hypersonic vehicle, thermal protection system

1. Introduction

Mars attracted human attention since 1960. To understand the importance of Mars exploration, several reasons should be considered. First, the Red Planet has similar dimensions compared to Earth's continental surfaces. Secondly, it has the capability to host Earth-like ecosystems promoting bacterial life. Furthermore, it represents a prototype sample to study the effects of a probable dramatic climate change [1].

Although the current Martian atmosphere is quite unfeasible for human life, the fundamental component for life i.e., water does exist on Mars around the poles and is probably distributed under the Martian surface. Therefore, a permanent human presence for research purposes on Mars requires reliable and affordable entry vehicles.

Several missions were performed in the past but unfortunately, most of them were unsuccessful [2, 3]. The first attempt to reach Mars was performed by URRS in 1960 with *Marsnik 1*. After several failures just on July 15th, 1965, the NASA *Mariner 4* successfully performed the first Mars flyby. Only in 1976 with *Viking 1* and *2* missions, for the first time, a human device successfully landed on Mars. On 4th July 1997, the first rover, *Pathfinder*, landed on Mars. The purpose of *Pathfinder* was to reduce the costs of space missions. It cost only 5% of *Viking* missions and was developed to test new technologies and approaches for future Mars missions.

During the last decades, significant technological advances have been done. NASA *Pathfinder* successors, *Spirit* and *Opportunity*, provided more than 100,000 images. Currently, three NASA rovers are active on the Martian surface: *InSight, Curiosity*, and *Perseverance*. *InSight* is currently devoted to study the planet's interior; while *Curiosity*, launched in 2012, is still operating on the Gale crater. Finally, Perseverance is the rover of the Mars 2020 mission, and its work objective is to look for signs of ancient life and collect rock and soil samples for a possible return to Earth (i.e., Mars sample return missions) [2]. This mission has the additional record of having allowed a small helicopter, namely Ingenuity, to fly to Mars for the first time in history.

All current Martian devices are unmanned [2]. However, for the upcoming Martian manned missions, recent studies have shown the limited possibility to adopt aeroshells for Mars landing. Braun and Manning [3] highlighted that without a lifting entry, Mars exploration with manned missions can result unfeasible because of the high g-loads associated with hypersonic deceleration and the touch-down.

In this work, a preliminary feasibility analysis of a Martian entry, performed with a lifting body having a blended double delta-wing, is performed. As no previous experience is gained on the use of lifting bodies for Mars entry, a conceptual configuration for an Earth re-entry mission from LEO is preliminarily assumed. A three degree of freedom (dof) trajectory model with a standard Mars atmosphere is adopted to address the entry and descent flight. A simplified heat transfer analysis based on the radiative equilibrium hypothesis for the wall of the descent spacecraft is also performed to compute heat loads during entry. The feedback on a trajectory, obtained by varying AoA and bank angle considering aerodynamic efficiency, and the capability to reach a predefined landing spot is discussed. The possibility to perform a lower deceleration within a shallower entry angle, taking full advantage of the Mars atmosphere is considered.

2. Lifting entry in Martian atmosphere

In 2007 NASA developed a standard design for a reference vehicle architecture for human Mars entry descent and landing (EDL) [4]. It consisted of a hypersonic aero assist entry system with a mid (0.6–0.8) Lift-to-Drag ratio (L/D) aeroshell, able to perform the aerobraking maneuver, that is ejected at a low supersonic Mach number. The use of hypersonic inflatable aerodynamic decelerators (HIADs) is also deeply studied to deliver human-class payloads to the surface of Mars [5]. However, inflatable decelerators do not provide sufficiently low terminal speed adequate for a safe manned landing [6, 7].

Recent studies highlighted the necessity to adopt a different vehicle design for manned missions [2]. A decisive design criterion is represented by the altitude at which the vehicle reaches a subsonic speed. Therefore, lifting body architectures having higher aerodynamic efficiency compared to aeroshells, are currently investigated for a high lift EDL mission [8, 9].

Specifically, lifting bodies (like Dream Chaser) allows a more favorable aerothermal environment and can customize the landing spot using bank angle modulation [10]. Control authority is also important for Mars explorations because it opens the possibility of using a lightweight Thermal Protection System (TPS). Besides, heat load can be controlled with drag (i.e., AoA) modulation which varies the ballistic coefficient during the entry phase according to a prescribed guidance law. Therefore, unlike capsules, a lifting body can take advantage of the

Mars atmosphere, albeit a very thin one, thus reducing the peak heat rate and g-loads.

Although the above-mentioned aspects seem very promising, several issues have to be considered. First, Mars atmosphere is very different from the Earth's one, and past and present lifting body "know-how" is only related to Earth missions. Furthermore, current vehicles prototypes have not performed a complete re-entry from space yet, not even on Earth. Additionally, because of superior aerodynamic performances, the lifting vehicle would tend to skip out because of the thinner Martian atmosphere. Therefore, to perform a conventional entry and descent maneuver, a very shallow entry angle needs to be adopted [4]. Low flight-path angles are preferred in order to achieve a lower terminal velocity to ensure a safe landing phase.

3. Concept vehicle for Mars entry, descent, and landing

To date, lifting body architectures have not been employed yet for Mars EDL missions. Therefore, only *a-priori* knowledge based on Earth re-entry vehicles can be assumed. In this work, a conceptual lifting body configuration, suitable for a manned entry mission starting from a Mars low orbit is considered [8, 9]. The vehicle is derived from a design procedure supported by a multidisciplinary optimization (MDO) analysis. By accounting in the design loop several sub-disciplines, a blended wing body with a double-delta planform configuration with low wing loading, and capable to perform a long gliding trajectory (i.e., $\gamma \ll 1^{\circ}$) can be derived (**Figure 1**) [9, 10].

The vehicle is designed to exploit a specific guidance law modulating the AoA versus Mach number in order to attain a favorable value of convective heat flux profile and promote the cooling down of the passive TPS exclusively by thermal radiation.

Reference geometric parameters of vehicle are shown in **Table 1**.

Figure 1.
Entry vehicle representation.

Parameter	Value
Nose radius (R_n)	0.47 m
Reference surface (S_{ref})	44.6 m^2
Mass (m)	12,105 kg
Wall emissivity (ε)	0.8
BC	452 kg/m^2

Table 1.
Entry vehicle parameters.

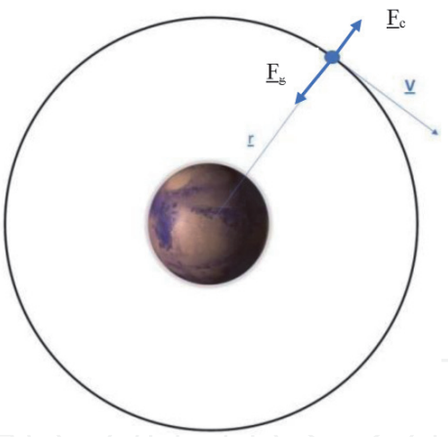

Figure 2.
Initial conditions of entry trajectory.

4. Overall mission specification

The Mars entry flight is described assuming a point mass model, starting from a low circular orbit. The orbit condition implies the equilibrium between centrifugal and gravity force, see **Figure 2**, given by $F_c = \frac{mv^2}{r}$ and $F_g = G\frac{M_{Mars}m}{r^2}$:

$$G\frac{M_{Mars}m}{r^2} = \frac{mv^2}{r} \tag{1}$$

where $r = R_{Mars} + h_0$ and $G = 6.673 \times 10^{-11}\frac{Nm^2}{kg}$, being R_{Mars} the planet radius and h_0 = 120 km the entry altitude.

Using the geometric data for the vehicle, the initial entry speed from Eq. (1) can be obtained:

$$V(t_0) = \sqrt{\frac{G \bullet M_{Mars}}{R_{Mars} + h_0}} = 3484m/s \tag{2}$$

Initial flight path angle γ_0 is an important design parameter for entry vehicles. For the sake of simplicity, the other initial conditions are chosen as follows:

$$\chi(t_0) = 0\ rad; \theta(t_0) = 0\ rad\varphi; (t_0) = 0\ rad \tag{3}$$

It is supposed that below $M_\infty = 2$ a supersonic inflatable decelerator performs the final deceleration to the terminal landing speed and a paraglider allows the touchdown.

5. Martian atmosphere model

To evaluate the descent trajectory of the lifting body, a proper model of the Martian atmosphere is adopted. In the present computations, the General Circulation Model (GCM) is assumed. GCM provides Mars atmosphere properties according to average data available by past exploration missions on the Red Planet. Atmospheric values of temperature, pressure, and density up to 125 km of altitude (see **Figure 3**) are obtained with the Mars Climate Database (MCD) which allows also small-scale meteorology predictions of storms and seasonal winds [11].

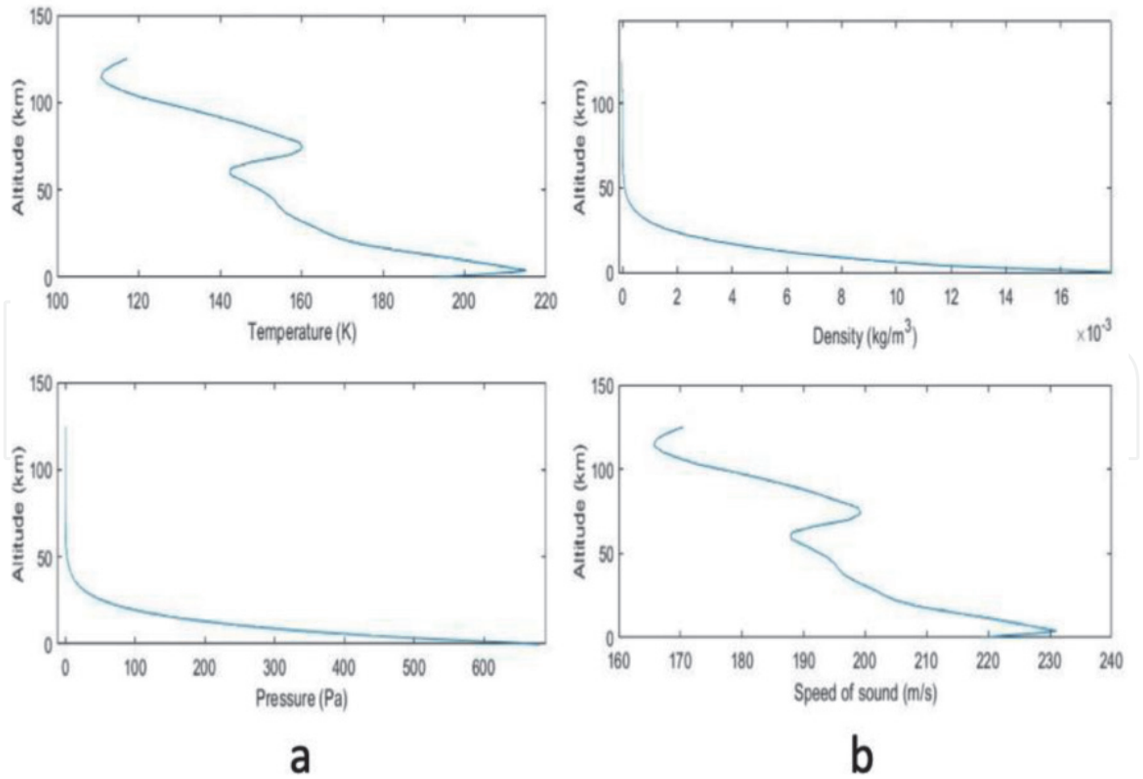

Figure 3.
Martian atmosphere: temperature and pressure (a); density and speed of sound (b).

6. Aeroheating

During most of the entry phase, the vehicle flies at hypersonic speeds. For instance, the aeroshell which landed the NASA rover *Curiosity*, started its descent on Mars at 125 km of altitude, at speed of 5800 m/s [12]. Using the MCD model at 125 km, a M_∞ = 34 is obtained. At such high Mach numbers, shock waves and turbulent boundary layers determine very high aerothermal loading conditions (i.e., large radiative and convective heat fluxes, and pressure loads) for the vehicle.

As it is well known, vehicle aeroheating is strictly related to the kind of entry trajectory. Shallower entry leads to a smaller heat rate, but increases the integrated heat loads, thus requiring a thicker TPS. Conversely, steep entries determinate higher heat rates and lower total heat loads. Therefore, in order to adopt a light-weight (passive) and fully reusable TPS, AoA and the flight-path angle are key parameters to trade-off thermal heating and vehicle mass (terminal landing speed).

Generally speaking, the first law of Thermodynamics states that during the descent, the huge amount of kinetic energy (KE) and potential energy (PE) of an entry vehicle dissipate into heat energy that warm up both spacecraft and the atmosphere surrounding it.

Moreover, heat transfer is mutually exchanged between the vehicle surface and the surrounding flow through convection and radiation. The energy balance at spacecraft wall suggests that the convective heat flux, $\dot{q}_{conv}$, is given by the sum of heat conducted into the TPS material, $\dot{q}_{cond}$, minus the amount of heat reradiated, $\dot{q}_{rad}$. By neglecting the conduction inside the heatshield, we have:

$$\dot{q}_{conv} = \dot{q}_{rad} \tag{4}$$

being $\dot{q}_{conv} = 7.207x10^4 \frac{\rho_\infty^{0.47}}{R_n^{0.54}} v^{3.5}$ (W/m^2), given by the Sutton-Graves stagnation-point relationship, and $\dot{q}_{rad} = \sigma\varepsilon T_w^4$, according to the

Stephan-Boltzmann law. Thus, for a safe landing, this huge heat energy must be transferred to the spacecraft shock-layer (i.e., surrounding gas instead of spacecraft) as much as possible.

The heat that goes to the vehicle during time dt is given by the product of heat flux rate, $\dot{q}$, and the reference aerodynamic surface of the vehicle:

$$\frac{dQ}{dt} = \dot{q} S_{ref} \tag{5}$$

which can be re-written as:

$$\dot{q} = \overline{St} \rho_\infty v_\infty \left[\frac{v_\infty^2}{2} + c_p \left(T_\infty - \overline{T}_w \right) \right] \tag{6}$$

where $\overline{St}$ is a mean Stanton number, $\overline{T}_w$ is a vehicle mean temperature and T_∞ is the freestream temperature. Neglecting the thermal contribution $c_p(T_\infty - \overline{T}_w)$, and substituting in (5) one has:

$$dQ = \overline{St} \rho_\infty \frac{{v_\infty}^3}{2} S_{ref} dt \tag{7}$$

Vehicle acceleration related to ballistic coefficient reads:

$$m \frac{dv}{dt} = -\frac{1}{2} \rho v^2 \mathrm{c}_D \, \mathrm{S}_{ref} \tag{8}$$

Therefore, by replacing S_{ref} given by Eq. (8) in Eq. (7) and integrating over time between initial speed, v_i, and the current one at time t, v, it follows:

$$\Delta Q = \frac{\overline{St}}{2 C_D} m \left(v_i^2 - v^2 \right) \tag{9}$$

Eq. (9) expresses the integrated heat load absorbed by the vehicle during the descent in the time interval $[t_i, t]$. Here, spacecraft energy is represented only by KE. Anyway, this approximation can be accepted considering that the PE of entry vehicle is negligible if compared with KE.

According to Eq. (9), the fraction of spacecraft energy that converts into vehicle heating (i.e., ΔQ) depends on the $\overline{St}/c_D$ ratio. Therefore, entry flights with high drag aeroshape (e.g., capsule aeroshapes) are suggested. This design solution, however, is not suitable for manned missions.

High lift configurations must be exploited in order to limit inertial loads and aerothermal loads by flying as much as possible shallow trajectory at higher altitudes, i.e. lower density. However, shallow entries ($\gamma \ll 1$ and $\alpha < 30^\circ$) are characterized by large flight time and consequently large integrated heat loads (ΔQ).

7. Entry dynamics

Mars entry trajectory is computed in a non-rotating, inertial, Mars-Fixed Mars-Centered reference frame [13]. A three degree-of-freedom numeric simulation is assumed, and the spacecraft is described as a point mass, performing a non-planar unpowered descent trajectory with a constant bank angle (**Figure 4**) [13]:

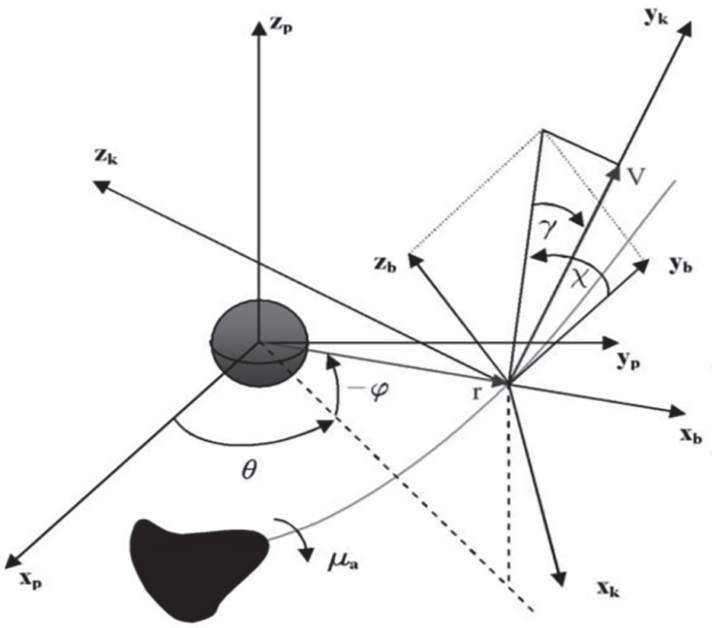

Figure 4.
Reference frames for entry flight equations.

$$\begin{aligned}
\frac{dV}{dt} &= -\frac{D}{m} - g\sin\gamma \\
\frac{d\gamma}{dt} &= \frac{1}{V}\left(\frac{L}{m}\cos\mu_a - g\cos\gamma + \frac{V^2}{r}\cos\gamma\right) \\
\frac{d\chi}{dt} &= \frac{1}{V}\left(\frac{L}{m}\frac{\sin\mu_a}{\cos\gamma} - \frac{V^2}{r}\cos\gamma\cos\chi\tan\varphi\right) \\
\frac{dr}{dt} &= V\sin\gamma \\
\frac{d\theta}{dt} &= \frac{V\cos\gamma\cos\chi}{r\cos\varphi} \\
\frac{d\varphi}{dt} &= \frac{V\cos\gamma\sin\chi}{r}
\end{aligned} \tag{10}$$

where θ, φ are the longitude and latitude in a spherical frame of reference, χ is the heading angle and μ_a is the bank angle.

Lift and Drag force are given by $L = \frac{1}{2}\rho V^2 S_{ref} C_L$ and $D = \frac{1}{2}\rho V^2 S_{ref} C_D$ respectively where aerodynamic coefficients C_L and C_D are taken using an aerodynamic database in hypersonic and low supersonic regimes [10].

The first order ODE system is integrated over time with a fourth-order explicit Runge–Kutta method.

8. Mars entry and descent flight

8.1 Entry with no bank modulation

Mars lifting entry is studied assuming the initial conditions expressed by Eq. (3):

$$V_e = 3484\, m/s; \gamma_e = -0.3^{\circ}; \mu_a = 0^{\circ}; \alpha_e = 20^{\circ}; 30^{\circ}; 45^{\circ} \tag{11}$$

Limits	Values
q_{max}	2000 Pa
n_{max}	0.5 terrestrial g's
Q_{max}	100 kW/m^2

Table 2.
Loads constraints.

In **Table 2** the structural and aerothermal constraints which define the entry corridor are shown.

The descent analysis is first performed at zero bank-angle to compute the nominal vehicle trajectory. With $\mu_a = 0^\circ$ the downrange distance depends only on aerodynamic efficiency (i.e., AoA modulation). In **Figure 5a** the effect of AoA on the entry trajectory is shown.

As α increases, the drag coefficient rises and the descent trajectory sinks more, thus moving to lower altitudes, see **Figure 5b**.

Looking at **Figure 5b** we see that with α = 20° the vehicle reaches M_∞ = 2 at an altitude of about 10 km higher than the case at α = 45°. At α = 20°, the spacecraft features a higher hypersonic aerodynamic efficiency. Therefore, higher L/D values appear more convenient for Mars missions to limit the terminal landing speed allowing at the same time a greater total range.

Figure 5c-5d confirms the advantage of flying with a high L/D. Long entry time (one-hour order-of-magnitude) could also help with the landing spot customization. However, for lifting bodies, increasing L/D leads to an increase of flight time (see **Figure 5d**), and integrated heat loads, see Eq. (5).

Finally, **Figure 5e-5f** show the effect of α on the peak heat flux rate and on its time history. At $\alpha = 45^\circ$ the peak heat flux is 90 kW/m^2, while decreases to 50 kW/m^2 at $\alpha = 20^\circ$. Therefore, the thermal peak is reduced, and non-ablating (re-usable) materials can be adopted. On the other hand, the longer flight time requires high emissivity materials to decrease heat transfer by conduction. In **Table 3** it is shown the total energy absorbed during entry.

In **Figure 5c** it is shown that for $\gamma = -0.3^\circ$ entry times are of the order of 10^4 s. To reduce entry flight time, steeper flight-path angles can be considered, see **Figure 6**.

Assuming $\gamma = -2.4°$, entry times are of the order of 10^3 s which can be compared to Earth re-entry flight time. However, progressively decreasing γ the peak heat flux rises (see values attained at $\gamma = -2.4°$). Therefore, a trade-off study between entry time and flight path-angle suggests the appropriate value related also to thermal insulation material capabilities.

8.2 Entry with bank angle modulation

Aerodynamic efficiency can be varied implicitly without using AoA modulation opportunely changing the bank angle μ_a. Bank modulates the lift force into two components $L_{eff} = L\ \cos\mu_a$ and $L_{side} = L\ \sin\mu_a$. The lateral force, L_{side}, deviates the lift vector outside the plane of trajectory, thus allowing a cross-range performance in the lateral direction. Therefore, trajectory footprint can be decomposed into two components: the down-range $\Delta x_p \sim \frac{L}{D}\ cos\,\mu_a$ and the cross-range $\Delta y_p \sim \frac{L}{D}\ sin\,\mu_a$. In **Figure 7** the effect bank modulation on vehicle trajectory is shown.

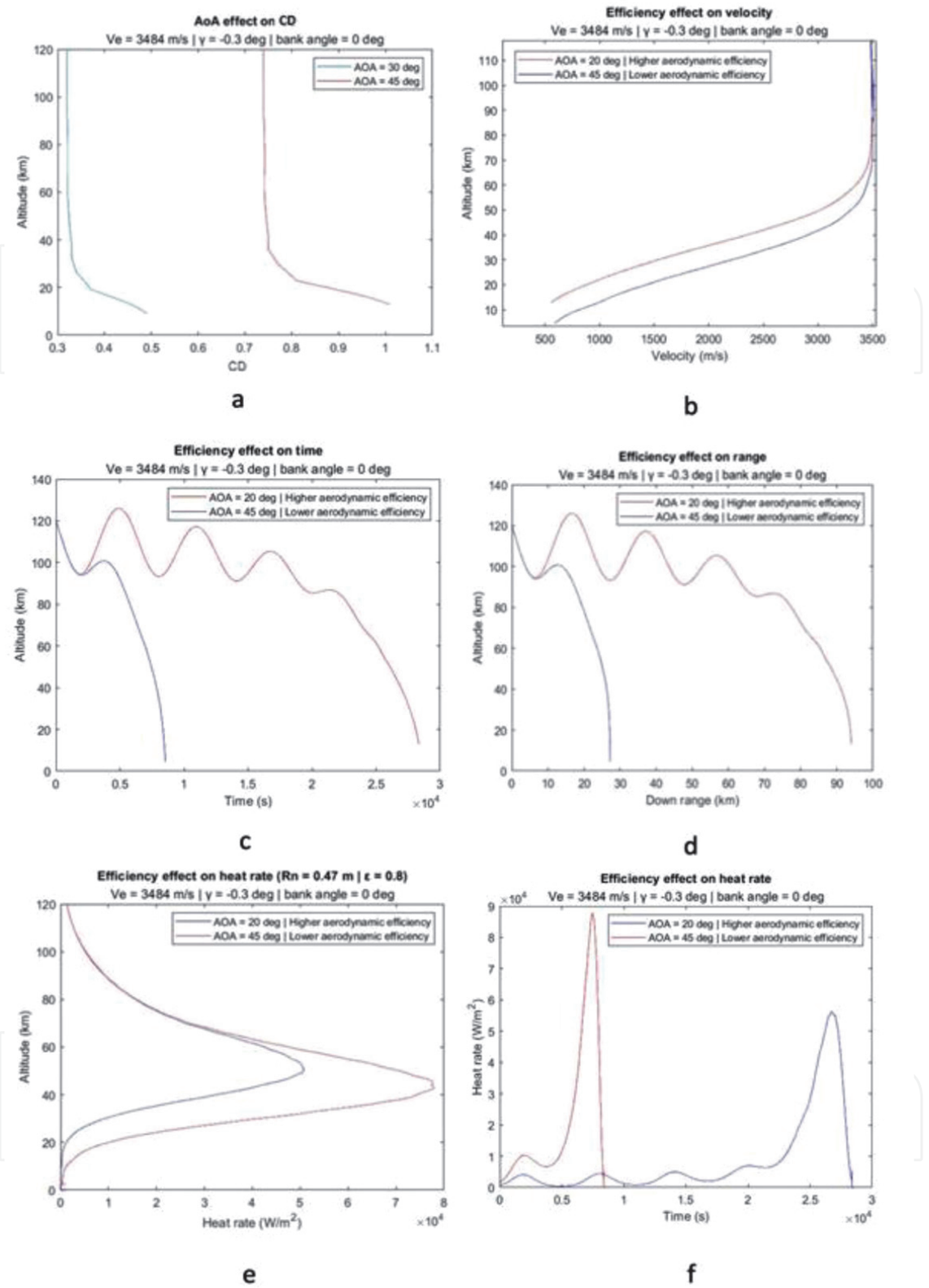

Figure 5.
Entry analysis with no bank angle modulation.

AoA (deg)	Total heat load (MJ/m^2)
20	374.72
45	113

Table 3.
Total energy absorbed during entry.

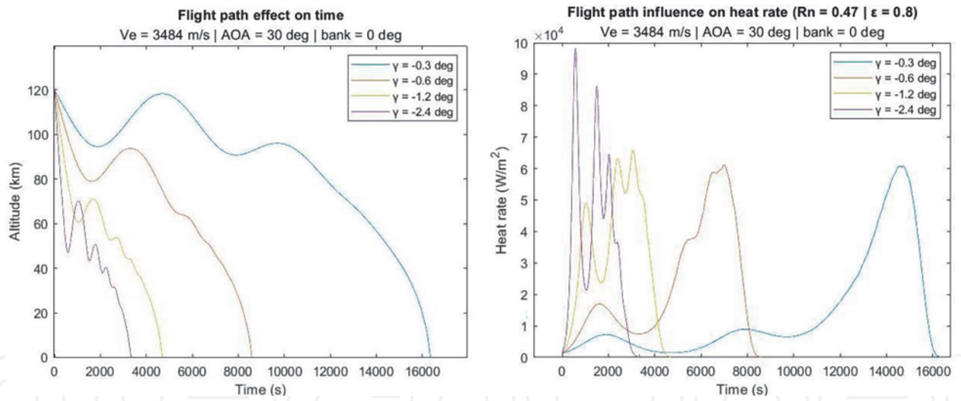

Figure 6.
Trade-off effects of flight path angle for entry flight at v_e = 3484 m/s, α = 30°, μ_a = 0°.

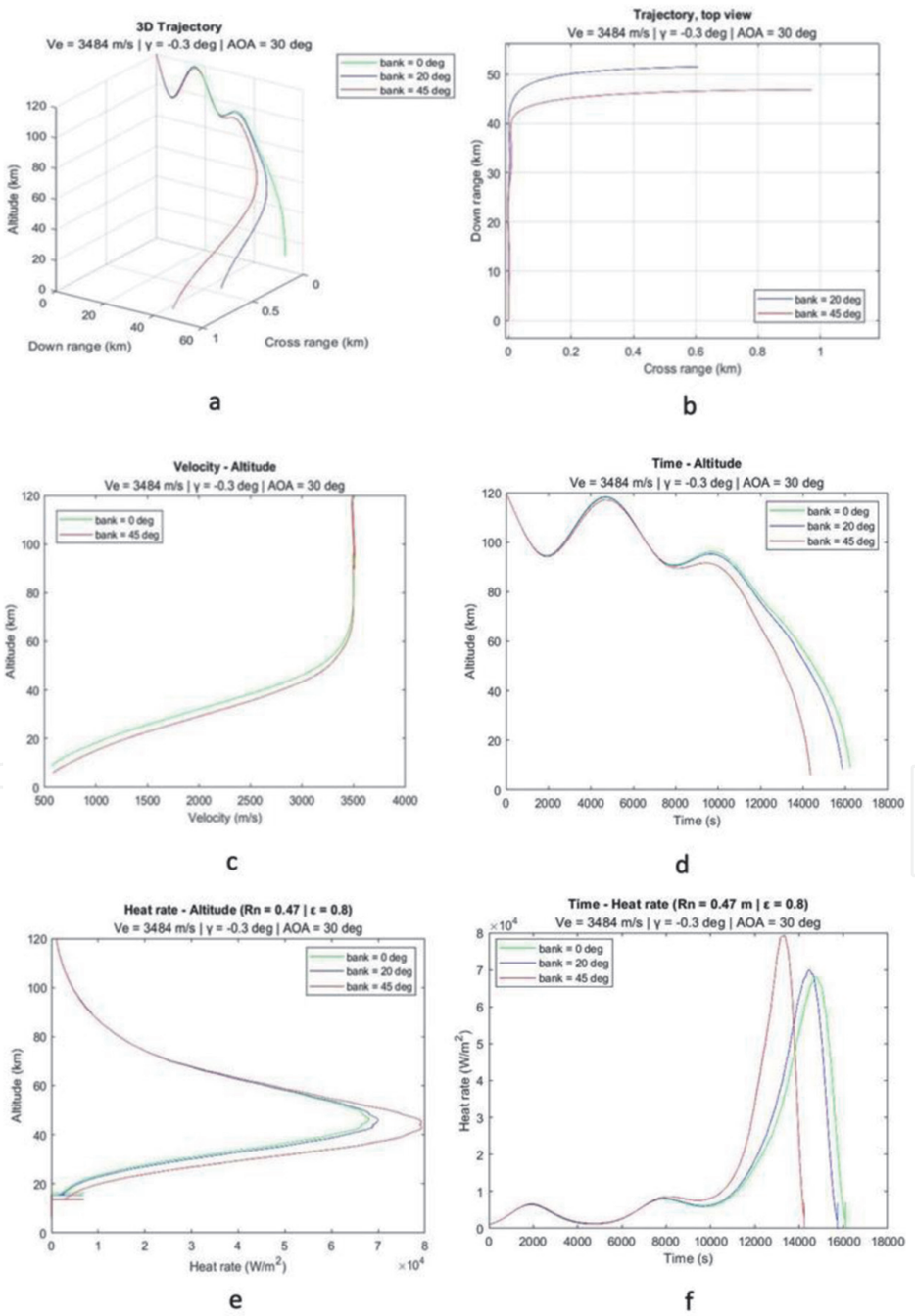

Figure 7.
Entry trade-off analysis with bank angle modulation.

Bank angle (deg)	Total heat load (MJ/m^2)
0	226.34
20	220.95
45	198.88

Table 4.
Total energy absorbed during re-entry.

Increasing μ_a at constant AoA (i.e., constant L/D) the total range (cross-range and downrange) increases. The effective lift component L_{eff} is reduced, and the vehicle attains a lower altitude at $M_\infty = 2, \mu_a = 20^\circ$ with respect to $\mu_a = 40^\circ$ as it is shown in **Figure 5c**. Therefore, control authority increases at expense of a higher terminal speed. Another effect of bank angle modulation can be observed in **Figure 7d**. The lower lift reduces the skip motion when the vehicle encounters the Martian atmosphere. Higher heat flux peaks over a shorter entry time are experienced. Therefore, at constant AoA, bank modulation improves the capability to reach the predefined landing spot.

Finally, in **Table 4** the total energy absorbed during the entry with bank modulation is computed.

From an energetic point of view, bank modulation toward higher μ_a favors lower total energy stored but shifts trajectory toward a ballistic-like behavior.

9. Conclusions

In this work, the feasibility of Mars entry with a lifting body was studied. Aerodynamic efficiency control is studied with respect to AoA and bank angle modulation. Decreasing AoA during Mars entry allows to reduce the peak heating, consequently increasing the flight-time. However, higher control on trajectory can be performed with bank angle modulation, which reflects over a higher control on the landing point, as well as the possibility to have a cross range. Furthermore, higher efficiency allows the vehicle to decelerate more at a higher altitude, taking advantage of the thin atmosphere. This is a crucial aspect for Mars missions in order to limit the terminal speed within allowable values for manned missions. Deceleration allows more tolerance on parachute deployment. Another benefit of a lifting vehicle is the influence on heat rate and total heat load: by increasing the aerodynamic efficiency, the heat rate peak can be decreased. The longer flight time induces the vehicle to store a higher amount of energy from the atmosphere, increasing the total heat load. Therefore, bank modulation can be performed assuming a suitable guidance law that modulates the vehicle aero-thermal loads inside the predefined constraints.

Acknowledgements

This work was supported by Universitá della Campania: “Luigi Vanvitelli”.

Conflict of interest

The authors declare that there is no conflict of interest regarding the publication of this chapter.

IntechOpen

Author details

Andrea Aprovitola, Fabrizio Medugno, Giuseppe Pezzella*, Luigi Iuspa and Antonio Viviani
Department of Engineering, University of Campania "L. Vanvitelli", Aversa, Italy

*Address all correspondence to: giuseppe.pezzella@unicampania.it

IntechOpen

References

[1] Genova A. Oracle: A mission concept to study Mars' climate, surface and interior. Acta Astronautica. 2020;**166**: 317-329

[2] NASA. Mars 2020 Perseverance Rover. 2020. Available from: https://www.mars.nasa.gov/programmissions/missions/future/mars2020

[3] Braun RD, Manning RM. Mars exploration entry, descent and landing challenges. Journal of Spacecraft and Rockets. 2007;**44**(2):310-323

[4] Mall K, Michael JG. High mass Mars exploration using slender entry vehicles. In: AIAA Atmospheric Flight Mechanics Conference. Reston, VA: American Institute of Aeronautics and Astronautics; 2016. DOI: 10.2514/6.2016-0019. Available from: https://arc.aiaa.org/doi/abs/10.2514/6.2016-0019

[5] Sostaric R. The Challenge of Mars EDL (Entry, Descent, and Landing). NASA JSC-CN-20470. Houston, TX, United States: NASA Johnson Space Center; Apr. 2010

[6] Lu Y. Aerocapture, aerobraking, and entry for robotic and human Mars mission. In: Pezzella G, Viviani A, editors. Mars Exploration A Step Forward. IntechOpen; 2020. DOI: 10.5772/intechopen.93281

[7] Viviani A, Iuspa L, Aprovitola A. Multi-objective optimization for re-entry spacecraft conceptual design using a free-form shape generator. Aerospace Science and Technology. 2017;**71**:312-324

[8] Lafleur JM, Cerimele CJ. Angle of attack modulation for Mars entry terminal state optimization. In: AIAA Atmospheric Flight Mechanics Conference; 10–13 August 2009. Chicago. Aerospace Research Central. Reston, VA: American Institute of Aeronautics and Astronautics; 2009

[9] Aprovitola A, Montella N, Iuspa L, Pezzella G. An optimal heat-flux targeting procedure for LEO re-entry of reusable vehicles. Aerospace Science and Technology. 2021;**112**:106608

[10] Viviani A, Aprovitola A, Iuspa L, Pezzella G. Aeroshape design of reusable re-entry vehicles by multidisciplinary optimization and computational fluid dynamics. Aerospace Science and Technology. 2020;**105**:106029

[11] Mars Climate Database (Web interface). 2016. Available from: http://www-mars.lmd.jussieu.fr/

[12] NASA. Final Minutes of Curiosity's Arrival at Mars. 2010. Available from: https://www.nasa.gov/mission_pages/msl/multimedia/gallery/pia13282.html

[13] Hirschel EH, Weiland C. Selected Aerothermodynamic Design Problem of Hypersonic Flight Vehicles. Berlin Heidelberg: Springer; 2009